Ligands for Oxovanadium(IV): Bis(catecholamide) Coordination and *Inter*molecular Hydrogen Bonding to the Oxo Atom

Torin M. Dewey, Justin Du Bois, and Kenneth N. Raymond*

Chemistry Department, University of California at Berkeley, Berkeley, California 94720

Received October 6, 1992

As a first step in the design of ligands which will bind selectively the vanadyl (VO^{2+}) ion, the syntheses of two 1,3-bis(2,2′-diethyl)benzene-linked bis(catecholamide) ligands and their corresponding oxovanadium(IV) complexes are described. The ligands form 1:1 ligand:VO^{2+} complexes which exhibit similar spectroscopic properties; vis/UV spectra and EPR parameters are characteristic of bis(catecholato) coordination. The complexes also show similar quasi-reversible electrochemical behavior for the V^{V}/V^{IV} redox couple. The structures of the VO^{2+} complexes of both 3,5-bis[2-(2,3-dihydroxybenzamido)ethyl]phenol (**1**) (designed to be capable of hydrogen bonding to VO^{2+}) and the comparison of 1,3-bis[2-(2,3-dihydroxybenzamido)ethyl]benzene (**2**) (with no hydrogen bond capability) have been determined. The solid-state structure of $K_2[VO(\mathbf{1})]\cdot 3C_3H_7NO$ reveals an *inter*molecular hydrogen bond to the vanadyl oxo atom between symmetry-related complexes. This hydrogen bond weakens the V=O bond and results in a change in the coordination sphere for the solid-state structure relative to the $[VO(\mathbf{2})]^{2-}$ complex. The complex $K_2[VO(\mathbf{1})]\cdot 3C_3H_7NO$ crystallizes in the space group $P2_1/n$ (No. 14) with unit cell parameters a = 13.644(3) Å, b = 16.643(5) Å, c = 16.753(2) Å, β = 99.13(1)°, V = 3756(2) Å^3, and Z = 4; R (R_w) = 3.6 (4.3)% for 478 parameters and 3995 reflections with $F_o^2 > 3\sigma(F_o^2)$. The complex $K_2[VO(\mathbf{2})]\cdot 3(C_3H_7NO)$ also crystallizes in $P2_1/n$ with unit cell parameters a = 13.844(4) Å, b = 17.633(7) Å, c = 16.410(4) Å, β = 108.07(2)°, V = 3808(2) Å^3, and Z = 4; R (R_w) = 5.1 (6.6)% for 482 parameters and 3572 reflections with $F_o^2 > 3\sigma(F_o^2)$.

Introduction

Selectivity of metal ion binding has increasingly been a goal of coordination chemists and a subtopic of the general field of molecular recognition. Early examples of metal-ion-selective ligands include the elegant contributions of Pedersen,[1] Lehn,[2,3] and Cram.[4,5] These crowns, spherands, coronands, etc. were designed largely on the basis of incorporating the appropriate donors for a metal ion around a fixed volume (rigid circular or spherical) cavity. Since metal cations often can be viewed in terms of a hard sphere model, recognition can be based solely on charge and size considerations. Such a model works well for the alkali metals and alkaline earth cations,[6] rare earth cations,[7] and even transition metal cations such as Fe^{3+},[8] or actinide cations such as Pu^{4+}.[9] However, metal oxo cations (e.g. VO^{2+}, TcO^{3+}, UO_2^{2+}, OsO_2^{2+}, etc.) clearly cannot be included in this group. The optimal design of ligands appropriate for these metal cations should include aspects which recognize the metal oxo moiety on the basis of geometrical properties, not solely the scalar properties of charge and size, what we have called stereognostic coordination chemistry.[10] Recently our efforts have been directed toward the design, synthesis, and metal ion coordination behavior of ligands tailored for various metal oxo cations.[11,12]

The metal oxo cations offer both unique challenges and opportunities for the rational design of metal-specific complexing agents. Although the oxo group can be thought of as a "blocked" coordination site, it is also a potential recognition site on the metal cation. Our approach to recognition of the oxo group is to design ligands which incorporate a hydrogen-bond donor within the framework of the ligand which can interact with the oxo group when the metal oxo species is bound. In this manner we can tailor ligands which not only bind the metal ion center through M–L interactions, but also recognize the metal oxo unit.

To establish the feasibility of this approach, it is important to determine whether the types of complexes we intend to study will take part in hydrogen bonding interactions and what tools are available to us to study this interaction. The oxo moieties of the UO_2^{2+} cation have been shown in numerous crystal structures to participate in intermolecular hydrogen-bonding interactions, with both solvent protons as well as protons on ammonium ions.[13,14] In addition, the oxo moiety of the VO^{2+} cation has been shown to participate in hydrogen bonding, in one case with solvent water protons,[15] and in another case with a phenolic proton of a co-crystalline 1,4-dihydroxybenzene molecule.[16] Although the vanadyl oxygen is less basic than water, there is evidence in the literature for significant electron density residing on the oxo group.[17,18] Our goal is the rational design and synthesis of metal-

* Author to whom correspondence should be addressed.

(1) Pedersen, C. J. *Angew. Chem., Int. Ed. Engl.* **1988**, *27*, 1021 and references therein.
(2) Lehn, J. M. *Struct. Bonding* **1973**, *16*, 1.
(3) Lehn, J. M. *Science* **1985**, *227*, 849.
(4) Cram, D. J. *Angew. Chem., Int. Ed. Engl.* **1988**, *27*, 1009.
(5) Cram, D. J.; Kaneda, T.; Helgeson, R. C.; Brown, S. B.; Knobler, C. B.; Maverick, E.; Trueblood, K. N. *J. Am. Chem. Soc.* **1985**, *107*, 3645.
(6) Lehn, J. M. *J. Inc. Phenom.* **1988**, *6*, 351.
(7) Yee, E. L.; Gansow, O. A.; Weaver, M. J. *J. Am. Chem. Soc.* **1980**, *102*, 2278.
(8) Raymond, K. N.; Garrett, T. M. *Coord. Chem. Rev.* **1988**, *105*, 135 and references therein.
(9) Raymond, K. N.; Garrett, T. M. *Pure Appl. Chem.* **1988**, *60*, 1807 and references therein.
(10) Stereognosis: "ability to perceive or the perception of material qualities (as form ...) of an object by handling ... tactile recognition," Webster's Third New International Dictionary, Unabridged, Springfield MA, 1986.
(11) Franczyk, T. S.; Czerwinski, K. R.; Raymond, K. N. *J. Am. Chem. Soc.* **1992**, *114*, 8138.
(12) Borovik, A. S.; Dewey, T. M.; Raymond, K. N. *Inorg. Chem.* **1993**, *32*, 413.
(13) (a) Perry, D. L.; Templeton, D. H.; Zalkin, A. *Inorg. Chem.* **1978**, *17*, 3699. (b) Perry, D. L.; Templeton, D. H.; Zalkin, A. *Inorg. Chem.* **1979**, *18*, 879. (c) Perry, D. L.; Zalkin, A.; Rube, H.; Templeton, D. H. *Inorg. Chem.* **1982**, *21*, 237. (d) Sarin, V. A.; Linde, S. A.; Fykin, L. E. *Russ. J. Inorg. Chem.* **1983**, *28*, 866. (e) Zalkin, A.; Ruben, H.; Templeton, K. H. *Inorg. Chem.* **1978**, *17*, 3701.
(14) Franczyk, T. S. Ph.D. Thesis, University of California at Berkeley, 1991.
(15) Tachez, M.; Theobold, F.; Hewat, A. W. *Acta Crystallogr. B* **1982**, *38*, 1807.
(16) Drew, M. C. B.; Mitchell, P. C. H.; Scott, C. E. *Inorg. Chim. Acta* **1984**, *82*, 63. Hydrogen bonding is assumed on the basis of the O–O distance of 2.82 Å.
(17) Yang, C. H.; Ladd, J. A.; Goedken, V. L. *J. Coord. Chem.* **1988**, *18*, 317.
(18) Cashin, B.; Cunningham, D.; Gallagher, J. F.; McArdle, P.; Higgins, T. *J. Chem. Soc., Chem. Commun.* **1989**, 1445.

0020-1669/93/1332-1729$04.00/0

specific ligands for both the VO^{2+} and UO_2^{2+} metal oxo species[11,12] as well as other metal oxo cations.[19,20] This paper, however, will focus on progress toward the design of appropriate ligands for the vanadyl ion.

The oxovanadium(IV) ion is ubiquitous in the coordination chemistry of vanadium(IV).[21] Numerous X-ray crystal structures containing the discrete VO^{2+} unit have been determined, resulting in a wealth of information about the coordination geometry around the vanadium center. Indeed, the V=O multiple bond generally remains intact following changes in the coordination of the metal center; a notable exception is the tris(catecholato)vanadium(IV) species, which can be prepared from vanadyl precursors.[22] The most common geometry observed is square pyramidal, with the vanadium sitting between 0.3 and 0.6 Å above the basal plane of the four equatorial donors. The average equatorial bond distances range from about 1.95 Å for O donors to about 2.05–2.12 Å for N donors.[23] Inspection of the stability constants of the VO^{2+} ion with various types of ligands indicates the general preference for hard, negatively charged oxygen donors to stabilize the high oxidation state.[24] In particular, the catecholate dianion forms exceedingly stable complexes with VO^{2+} ($\log[ML_2]/[M][L]^2 = 33.5$ for catecholate(2–)).[25]

On the basis of the above considerations, our ligand design incorporates two important features: (1) A pair of bidentate catecholate groups to bind strongly to the equatorial positions of a square-based pyramid around the oxovanadium(IV). (2) The presence of a phenolic proton donor in the backbone of the ligand to hydrogen bond to the vanadyl oxygen.

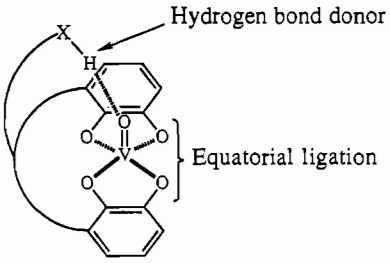

Initial efforts toward the design and synthesis of bis(catecholamide) ligands were based on polyamine backbones.

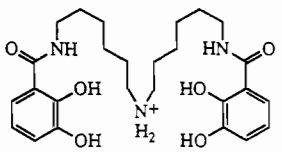

bicam6

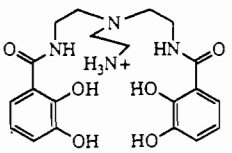

bicamtren

These were subsequently discarded in favor of the ligands shown, which follow this ligand design scheme: phencam, **1**, which

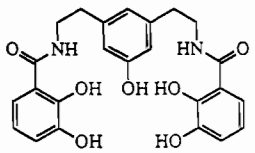

phencam, 1

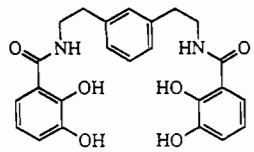

bencam, 2

incorporates a phenolic proton donor, along with the analogous ligand which lacks the phenol, bencam, **2**. The 1,3-bis(2,2′-diethyl)benzene linker arm which is employed in these ligands was designed to allow the two 2,3-dihydroxybenzamide (catecholamide, or **cam**) to approach the V(IV) metal center, while still allowing the phenol moiety to swing upward and sit axial to the oxo of the oxovanadium(IV). The syntheses of these ligands and the accompanying oxovanadium(IV) complexes as well as the spectroscopic and crystallographic characterization of the two metal complexes are described herein.

Experimental Section

General Methods. Metal complex syntheses were performed using standard Schlenk techniques under an argon or nitrogen atmosphere or in a homemade inert-atmosphere glovebox. Vanadyl acetylacetonate [$VO(acac)_2$] was recrystallized from acetone. Dicyclohexylcarbodiimide (DCC) was obtained from Fluka Chemical. Unless otherwise noted, all other starting materials were used without further purification as obtained from Aldrich Chemical Co. Methylene chloride (CH_2Cl_2), acetonitrile (CH_3CN), and methanol were distilled under a nitrogen atmosphere from calcium hydride. Tetrahydrofuran (THF) was distilled from sodium benzophenone ketyl under dry nitrogen. Other solvents were reagent grade unless otherwise noted. Thin-layer chromatographs (TLC) were performed using Analtech GHLF 250 μm silica on glass plates or Whatman KGF 250 μm silica on glass plates (2.5 × 10 cm and 5 × 10 cm, respectively) and visualized by fluorescence quenching at 254 nm. Flash chromatography was performed on Merck grade EM Science or Aldrich 230–400 mesh silica (Kieselgel 60). ^1H and $^{13}C\{^1H\}$-NMR were obtained on UCB 400 and 500-MHz Bruker spectrometers. Chemical shifts (δ) are reported in ppm downfield from tetramethylsilane (TMS) internal standard or referenced to solvent resonances. ^1H-NMR data are reported as δ value (multiplicity, integrated number of protons, and J values in Hz). IR data were obtained as KBr pellets or nujol mulls on KBr plates on a Nicolet 5DXB FTIR spectrometer and are reported in wavenumbers. Mass spectral data were obtained as positive ion fast-atom-bombardment (+FAB) m/e (intensity expressed as percent of base peak of 100%) using thioglycerol/glycerol (TG/G) or sulfolane as the matrix unless otherwise noted. Elemental analyses and mass spectra were performed by the Microanalytical Laboratory, College of Chemistry, University of California, Berkeley, CA.

Ligands. 3-(2,3-Dimethoxybenzoyl)-1,3-thiazolidine-2-thione (10). 2,3-Dimethoxybenzoic acid (8.01 g, 44.0 mmol) was dissolved in 250 mL of CH_2Cl_2 and the solution stirred vigorously. Dicyclohexylcarbodiimide (9.72 g, 47.1 mmol) was then added followed by the addition of 2-mercaptothiazoline (5.27 g, 44.0 mmol) and catalytic 4-dimethylaminopyridine (DMAP) (100 mg). The contents were allowed to stir for 24 h, and the white precipitate of *N,N′*-dicyclohexylurea filtered from the yellow solution, which was evaporated to a yellow oil. Excess 2-mercaptothiazoline was removed from the oil by successive extraction of a CH_2Cl_2 solution of the oil with 3 × 100 mL of 0.1 M NaOH. After drying the organic phase over anhydrous $MgSO_4$ and evaporation under reduced pressure, the yellow solid was recrystallized from $CHCl_3$/hexanes to give 9.97 g (80%) of yellow crystals, m.p. 123–124.5 °C. ^1H-NMR δ 7.07 (t, 1H, J = 7.9 Hz), 7.00 (dd, 1H, J_1 = 8.2 Hz, J_2 = 1.5 Hz), 6.90 (dd, 1H, J_1 = 7.7 Hz, J_2 = 1.5 Hz), 4.63 (t, 2H, J = 7.3 Hz), 3.92 (s, 3H), 3.87 (s, 3H), 3.41 (t, 2H, J = 7.3 Hz). $^{13}C\{^1H\}$-NMR δ 201.7, 168.0, 152.4, 146.1, 129.5, 124.1, 120.3, 115.1, 61.5, 55.9, 55.7, 29.2. Anal. Calcd (found) for $C_{12}H_{13}NO_3S_2$: C, 50.87 (51.03); H, 4.62 (4.81); N, 4.94 (5.06); S, 22.63 (22.71).

Dimethyl 5-Methoxyisophthalate (4). The title compound was prepared by a modified literature procedure.[26] 5-Methoxyisophthalic acid (3) (20.0 g, 106.5 mmol) was dissolved in 200 mL of dry, deoxygenated acetone under argon. Anhydrous K_2CO_3 (48.6 g, 3.1 equiv) was added to the reaction mixture, and dimethyl sulfate (44.3 g, 3.1 equiv) was

(19) Borovik, A. S.; Du Bois, J.; Raymond, K. N. To be submitted for publication.
(20) Borovik, A. S.; Dewey, T. M.; Raymond, K. N. To be submitted for publication.
(21) Cotton, F. A.; Wilkinson, G. *Advanced Inorganic Chemistry*, 5th ed.; Wiley-Interscience: New York, 1988.
(22) Cooper, S. R.; Koh, Y. B.; Raymond, K. N. *J. Am. Chem. Soc.* **1982**, *104*, 5092.
(23) As determined by a structure search on the Cambridge Structural Database, in which the vanadium had square pyramidal coordination geometry as follows: (1) the vanadium was five coordinate; (2) the angles from the oxo to the vanadium to the equatorial ligands were constrained to 100 ± 15°. Cambridge Crystallographic Data Center, Jan 1992 release. Note: the average $V-N_{eq}$ distances are 2.05 Å for oxovanadium(IV) with four nitrogens in the equatorial plane and 2.12 Å for mixed coordination in the equatorial plane (2 N, 2 O or 1 N, 3 O).
(24) Martell, A. E.; Smith, R. M. *Critical Stability Constants*; Plenum: New York, 1974–1989; Vols. 1–6.
(25) Martell, A. E.; Smith, R. M. *Critical Stability Constants*; Plenum Press: New York, 1977; Vol. 3, pp 201.
(26) Crandall, E. W.; Harris, L. *Org. Prep. Proc.* **1969**, *1*, 147.

added via syringe. The solution was brought to reflux for 12 h, then 15 mL of 10% KOH solution was added via syringe. After an additional four hours at reflux the solution was cooled, filtered, and evaporated under reduced pressure to afford a white solid which was recrystallized from MeOH/H_2O to give 21.8 g (91%) of white crystals, m.p. 110–112 °C (lit.[26] m.p. 111–111.5 °C). ^{1}H-NMR ($CDCl_3$) δ 8.27 (t, 1H, J = 1.4 Hz), 7.75 (t, 2H, J = 1.4 Hz), 3.94 (s, 6H), 3.89 (s, 3H). $^{13}C\{^1H\}$-NMR δ 166.0, 159.6, 131.7, 122.8, 119.2, 55.7, 52.3. Anal. Calcd (found) for $C_{11}H_{12}O_5$: C, 58.93 (58.74); H, 5.39 (5.35).

3,5-Bis(hydroxymethyl)anisole (5). This compound was also synthesized by a modified literature procedure.[27] In oven-dried apparatus under argon a solution of dimethyl 5-methoxyisophthalate (19.9 g, 89.2 mmol) in 50 mL of dried THF was added dropwise to a slurry of $LiAlH_4$ (14.0 g, 370 mmol) over 20 min, bringing the solution to reflux. The solution was kept at reflux by external heating for an additional 30 min, then allowed to cool. Slow addition of 14 mL of H_2O, 42 mL of 15% NaOH, and 14 mL of H_2O followed by filtration through a glass frit and evaporation of the solvents yielded a white solid, which was recrystallized from $CHCl_3$ to give 13.54 g (91%) of white needles, m.p. 67–69 °C (lit.[27] m.p. 67–68 °C). ^{1}H-NMR (d_6-acetone) δ 6.89 (s, 1H), 6.81 (s, 2H), 4.57 (d, 4H, J = 6.2 Hz), 4.18 (t, 2H, J = 5.9 Hz), 3.76 (s, 3H). $^{13}C\{^1H\}$-NMR δ 160.7, 144.7, 117.5, 111.1, 64.6, 55.3. Anal. Calcd (found) for $C_9H_{12}O_3$: C, 64.27 (63.68); H, 7.19 (7.05).

3,5-Bis(chloromethyl)anisole[28] (6a). To a solution of 3,5-bis(hydroxymethyl)anisole (**5**) (5.00 g, 29.7 mmol) in 80 mL of CH_2Cl_2 was added triethylamine (5 mL), followed by slow addition of a solution of freshly distilled thionyl chloride (8.9 g, 74.3 mmol, 2.5 equiv). The solution was then brought to reflux for 30 min, cooled, and 5 mL of MeOH in 20 mL of CH_2Cl_2 was added to decompose the remaining $SOCl_2$. The resultant solution was extracted with 2 × 100 mL of H_2O followed by 100 mL of brine, then dried over anhydrous Na_2SO_4 and evaporated under reduced pressure to a faintly yellow oil, which was dissolved in CH_2Cl_2 and eluted through a 19 × 80 mm flash silica plug and evaporated to give 5.42 g (89%) of the product as colorless needles, m.p. 51–52.5 °C. ^{1}H-NMR ($CDCl_3$) δ 6.99 (s, 1H), 6.88 (d, 2H, J = 1.3 Hz), 4.54 (s, 4H), 3.82 (s, 3H). $^{13}\{^1H\}$-NMR δ 160.0, 139.3, 120.8, 114.1, 55.4, 45.8. Anal. Calcd (found) for $C_9H_{10}Cl_2O$: C, 52.71 (52.74); H, 4.91 (4.92); Cl, 34.57 (34.44).

3,5-Bis(cyanomethyl)anisole (7a). A solution of 3,5-bis(chloromethyl)-anisole (**6a**) (4.30 g, 21.0 mmol) in 50 mL of CH_3CN was added dropwise to a slurry of potassium cyanide (**Caution**: extremely toxic, keep away from acid) (4.10 g, 3 equiv) and 18-crown-6 (1.11 g, 0.2 equiv) in 100 mL of CH_3CN, and the solution was allowed to stir overnight, resulting in the formation of a white precipitate. TLC (50% EtOAc/Hexanes) indicated that the reaction was not complete, so an additional 3.0 g of potassium cyanide was added, and the solution stirred for an additional 3 days. The reaction was quenched on 150 mL of ice-H_2O and extracted with 3 × 100 mL of CH_2Cl_2. These extracts were then extracted with 100 mL of dist. H_2O followed by 100 mL of brine, dried over anhydrous Na_2SO_4 and evaporated under reduced pressure to 3.6 g of a yellow oil, which was dissolved in EtOAc and passed through a 4 × 12 cm flash silica column eluted with 50% EtOAc/Hexanes. The eluant was evaporated under reduced pressure to give the product as 3.28 g (84%) of a colorless oil which solidified upon standing to give white crystals, m.p. 63–65.5 °C. ^{1}H-NMR ($CDCl_3$) δ 6.87 (s, 1H), 6.83 (s, 2H), 3.83 (s, 3H), 3.74 (s, 4H). $^{13}C\{^1H\}$-NMR δ 160.6, 132.2, 119.6, 117.3, 113.3, 55.5, 23.4. Anal. Calcd (found) for $C_{11}H_{10}N_2O$: C, 70.95 (70.65); H, 5.41 (5.41); N, 15.04 (14.70).

3,5-Bis(2-aminoethyl)anisole (8a).[29] 3,5-Bis(cyanomethyl)anisole (**7a**) (1.01 g, 5.4 mmol) was dissolved in 25 mL of glacial acetic acid, along with 155 mg of PtO_2 (15% by weight) in a stainless steel bomb. The solution was deoxygenated, pressurized to 500 psi H_2 and stirred at ambient temperature for 24 h. The solution was filtered through a glass frit, rinsed with acetic acid, H_2O, and EtOH, then coevaporated with ethanol twice, and reduced in vacuo to afford 3.02 g of a clear oil which was contaminated with HOAc. This oil was dissolved in 80 mL of 0.2 M HCl, and solid NaOH was added to pH > 13, 20 mL of brine was added, and the resultant solution extracted with 6 × 50 mL of CH_2Cl_2. The CH_2Cl_2 extracts were dried over anhydrous $MgSO_4$ and evaporated to give the product as a colorless oil, 0.79 g (75%). ^{1}H-NMR ($CDCl_3$) δ 6.64 (s, 1H), 6.61 (s, 2H), 3.79 (s, 3H), 2.96 (t, 4H, J = 6.9 Hz), 2.70 (t, 4H, J = 6.8 Hz), 1.37 (br s, 4H). $^{13}C\{^1H\}$-NMR δ 159.8, 141.4, 121.8, 112.1, 55.0, 43.3, 40.0. This compound was acylated in the next step without further purification.

3,5-Bis[2-(2,3-dimethoxybenzamido)ethyl]anisole (9a, Me_4phencam). 3,5-Bis(2-aminoethyl)anisole (**8a**) (1.40 g, 7.2 mmol) was dissolved in 50 mL of CH_2Cl_2. A solution of 3-(2,3-Dimethoxybenzoyl)-1,3-thiazolidine-2-thione (**10**) (4.08 g, 14.4 mmol) in 30 mL of CH_2Cl_2 was added and the solution brought to reflux for 30 min. TLC (5% MeOH/CH_2Cl_2) showed the presence of one major product at $R_f \sim 0.3$. The solution was cooled and extracted with 2 × 100 mL of 0.2 M HCl, 2 × 100 mL of 0.1 M NaOH, 100 mL of brine, then dried over anhydrous $MgSO_4$ and evaporated to give 4.1 g of an oil. This oil was chromatographed on a 5 × 18 cm silica column, eluted with 0–4% MeOH/CH_2Cl_2. Pure fractions were combined and evaporated to give the title compound as 3.44 g (91%) of a colorless oil. ^{1}H-NMR ($CDCl_3$) δ 8.06 (unres. t, 2H), 7.69 (dd, 2H, J_1 = 8.0 Hz, J_2 = 1.5 Hz), 7.12 (t, 2H, J = 8.0 Hz), 7.00 (dd, 2H, J_1 = 8.1 Hz, J_2 = 1.5 Hz), 6.78 (s, 1H), 6.69 (s, 2H), 3.88 (s, 6H), 3.79 (s, 3H), 3.75 (m, 4H), 3.68 (s, 6H), 2.90 (t, 4H, J = 7.0 Hz). $^{13}C\{^1H\}$-NMR δ 165.0, 160.0, 152.4, 147.4, 140.8, 126.5, 124.2, 122.6, 121.5, 115.1, 112.3, 60.9, 55.9, 55.1, 40.6, 35.4. +FAB mass spectrum m/e 545 (7%, M + Na^+), 523 (98%, MH^+), 341 (19%), 299 (23%), 241 (62%), 225 (88%), 165 (100%). Anal. Calcd (found) for $C_{29}H_{34}N_2O_7$: C, 66.65 (66.25); H, 6.56 (6.75); N, 5.36 (5.24).

3,5-Bis[2-(2,3-dihydroxybenzamido)ethyl]phenol (1, H_4phencam). Me_4-phencam (**9a**) (2.80 g, 5.4 mmol) was dissolved in 40 mL of dry CH_2Cl_2 and cooled 0 °C, then filtered through glass wool. A large excess of neat boron tribromide (33.6 g, 134 mmol) was added via syringe to the cooled, stirred reaction mixture, giving a viscous yellow solution. The reaction was stoppered and stirred for 4 days at ambient temperature, at which time the volatiles were removed in vacuo. The remaining light yellow solid was quenched with 100 mL of distilled H_2O and the solid transferred to a 1 L Erlenmeyer flask, along with 50 mL of methanol to remove the remainder of the solid. The solution was brought to reflux, the volume reduced to ca. 200 mL, and 200 mL of EtOAc was added to dissolve the brown oily residue. The layers were separated and the aqueous layer was extracted with an additional 3 × 200 mL of EtOAc, and the combined organics were dried over anhydrous $MgSO_4$ and evaporated to give 2.28 g (94% crude) of tan foamy solid. ^{1}H-NMR (d_6-DMSO) δ 8.87 (t, 2H, J = 5.3 Hz), 7.25 (dd, 2H, J_1 = 8.1 Hz, J_2 = 1.1 Hz), 6.89 (dd, 2H, J_1 = 7.8 Hz, J_2 = 1.2 Hz), 6.56 (s, 1H), 6.49 (s, 2H), 3.45 (m, 4H), 2.72 (t, 4H, J = 7.7 Hz). $^{13}C\{^1H\}$-NMR δ 169.6, 157.4, 149.7, 146.2, 140.5, 119.8, 118.7, 117.8, 117.1, 115.0, 113.5, 40.6, 34.9. IR (KBr pellet, cm^{-1}) 3500–3100 (br s), 1637 (vs), 1594 (vs), 1543 (vs), 1487 (m), 1461 (s), 1330 (br s), 1264 (br s), 1240 (sh), 1166 (m), 977 (w), 900 (w), 843 (w), 803 (w), 740 (m), 590 (m). +FAB mass spectrum m/e 475 (14%, M + Na^+), 453 (72%, MH^+), 317 (31%), 279 (18%). Analytically pure samples were prepared by slow evaporation of EtOH away from an EtOH/H_2O solution to give white crystals which were dried in vacuo (hygroscopic), m.p. > 170 °C. Anal. Calcd (found) for $C_{24}H_{24}N_2O_7$: C, 63.71 (63.45); H, 5.35 (5.33); N, 6.19 (6.14).

1,3-Bis(cyanomethyl)benzene (7b). An addition funnel was charged with α,α'-dichlorometaxylene (**6a**) (2.50 g, 14.3 mmol) in 20 mL of CH_3CN. The solution was added dropwise to a slurry of potassium cyanide (5.61 g, 86.1 mmol) and 18-crown-6 (0.75 g, 15% by wt.) in 100 mL of CH_3CN with vigorous stirring over 2 h. After stirring the reaction mixture overnight, the solution was quenched on a 100 mL ice-water mixture, and the mixture was extracted with 3 × 100 mL CH_2Cl_2. The CH_2Cl_2 extracts were collected, dried over anhydrous $MgSO_4$, and evaporated to a yellow oil, which was chromatographed on a 5 × 20 cm flash silica gel column with 20–40% EtOAc/hexanes. Pure fractions were combined and evaporated to give 1.90 g (85%) of the product as a pale yellow oil. ^{1}H-NMR (d_6-acetone) δ 7.36 (d, 1H, J = 8.8 Hz), 7.20 (m, 2H), 6.83 (t, 1H, J = 7.6 Hz), 2.91 (s, 4H). This compound was hydrogenated in the next step without further purification.

1,3-Bis[2-(2,3-dimethoxybenzamido)ethyl]benzene (9b, Me_4bencam). 1,3-Bis(cyanomethyl)benzene (**7b**) (1.90 g, 12.2 mmol) was dissolved in 20 mL of glacial acetic acid to which a catalytic amount of PtO_2 (0.30 g) was added. The mixture was stirred in a sealed bomb, the solution deoxygenated, and placed under 500 psi H_2. After allowing the contents to stir overnight the reaction mixture was filtered and quenched on 100 mL dist. H_2O, and the pH raised to 14 using conc. NaOH. The aqueous phase was extracted using 6 × 50 mL CH_2Cl_2. The CH_2Cl_2 extracts were collected, dried over anhydrous $MgSO_4$, and evaporated to give the 1,3-bis(2-aminoethyl)benzene (**8b**) precursor as a yellow oil (1.58 g, 80%

(27) Zimmerman, H. E.; Jones, G. *J. Am. Chem. Soc.* **1970**, *92*, 2753.
(28) 3,5-Bis(bromomethyl)anisole has been described previously (see ref 27) and was initially used for the synthetic scheme employed here, but the dichloride analogue **6a** was found to give better results in the next step of the synthesis (conversion to the dinitrile).
(29) Bergeron, R. J. *Synthesis* **1981**, 732.

crude yield). This oil was dissolved in 200 mL of CH_2Cl_2, and 3-(2,3-dimethoxybenzoyl)-1,3-thiazolidine-2-thione (**10**) (5.45 g, 19.2 mmol) was added to the stirred solution. After stirring overnight the solution had become colorless, indicating the completion of the reaction. The solution was extracted with 3 × 100 mL 0.1 M NaOH to remove the 2-mercaptothiazoline, and the organic phase was dried over anhydrous $MgSO_4$ and evaporated to a clear oil. The oil was eluted through a 7 × 10 cm silica gel plug in 5% $MeOH/CH_2Cl_2$ to remove baseline impurities, and the eluant evaporated to a clear oil which solidified upon standing to give 4.47 g (76% from dicyano compound) of the product as a colorless solid. ^{1}H-NMR ($CDCl_3$) δ 8.04 (unres. t, 2H), 7.69 (dd, 2H, J_1 = 8.0 Hz, J_2 = 1.5 Hz), 7.27 (d, 2H, J = 8.0 Hz), 7.18 (s, 1H), 7.14 (d, 1H, J = 8.1 Hz), 7.12 (d, 2H, J = 8.0 Hz), 7.00 (d [unres. dd], 2H, J = 7.6 Hz), 3.85 (s, 6H), 3.74 (m, 4H), 3.61 (s, 6H), 2.93 (t, 4H, J = 7.0 Hz). The compound was deprotected in the next step without further purification.

1,3-Bis[2-(2,3-dihydroxybenzamido)ethyl]benzene (2, H_4bencam). Me_4-bencam (**9b**) (2.03 g, 4.1 mmol) was dissolved in 200 mL of dry CH_2Cl_2. The solution was deoxygenated and stirred under an argon atmosphere. Neat boron tribromide (1.55 mL, 16.4 mmol) was added via syringe to reaction flask. The contents were allowed to stir for three days after which time the reaction was quenched with distilled H_2O (ca. 1500 mL) and the CH_2Cl_2–H_2O solution was brought to a boil. The insoluble light brown precipitate was filtered from the hot aqueous solution; the precipitate was judged to be pure by TLC (1% HOAc/5% $MeOH/CH_2Cl_2$). The product was recrystallized from a boiling $CHCl_3$/hexanes solution to give the product as a tan solid (1.49 g, 83%), m.p. > 170 °C. ^{1}H-NMR (d_6-acetone) δ 13.06 (s, 2H), 8.21 (unres. t, 2H), 7.68 (s, 2H), 7.23–7.18 (m, 4H), 7.10 (dd, 2H, J_1 = 7.5 Hz, J_2 = 1.3 Hz), 6.94 (dd, 2H, J_1 = 6.7 Hz, J_2 = 1.2 Hz), 6.68 (t, 2H, 8.0), 3.61 (m, 4H), 2.90 (t, 4H, J = 7.3 Hz). ^{13}C[^{1}H]-NMR δ 171.3, 150.9, 147.3, 140.3, 130.1, 129.4, 127.6, 119.2, 119.0, 117.4, 115.4, 41.8, 36.1. IR (KBr pellet, cm^{-1}) 3501 (s), 3339 (s), 2931 (w), 1631 (s), 1581 (s), 1550 (br s), 1469 (s), 1459 (s), 1322 (m), 1266 (s), 1234 (s), 1169 (s), 1061 (m), 894 (w), 844 (w), 816 (m), 750 (s), 709 (m), 666 (br m), 581 (w), 466 (s), 434 (w). Mass spectrum (E.I.) m/e 437 (33%, M^+), 301 (33%), 225 (33%). Anal. Calcd (found) for $C_{24}H_{24}N_2O_6 \cdot 0.25H_2O$: C, 65.37 (65.31); H, 5.60 (5.72); N, 6.35 (6.24).

Metal Complexes. K_2VO[phencam]. A solution of 0.50 M KOH in EtOH (1.00 mL, 0.50 mmol) was dissolved in 25 mL of EtOH. The ligand, H_4phencam **1** (0.100 g, 0.22 mmol) was added to the basic EtOH and the solution deoxygenated. The basic ligand solution was added to a solution of $VO(acac)_2$ (0.059 g, 0.22 mmol) in 25 mL of EtOH, resulting in an aqua green solution. This solution was stirred for 30 min and the solvent removed in vacuo. The green solid was dissolved in ca. 3 mL of MeOH and loaded onto a lipophilic Sephadex LH-20 (Sigma Chem.) column (19 mm × 15 cm) packed in MeOH, and eluted with MeOH. The prominent green band was collected and the solvent evaporated. The resultant green solid was recrystallized by diffusing Et_2O into a DMF solution (trace H_2O) of the complex, rinsed with Et_2O and allowed to dry under nitrogen, yielding 0.119 g (67%) of blue-green needles which were suitable for X-ray diffraction. IR (KBr pellet, cm^{-1}) 3237 (m), 3235 (m), 3073 (m), 3059 (m), 2951 (m), 2933 (m), 1660 (s), 1628 (s), 1590 (s), 1550 (s), 1460 (s), 1440 (s), 1412 (w), 1389 (m), 1296 (s), 1246 (s), 1215 (s), 1199 (m), 1099 (m), 1046 (m), 934 (m), 924 (s), 771 (m), 746 (m), 696 (m), 670 (m), 641 (m), 548 (m), 540 (m), 410 (m). Anal. Calcd (found) for $C_{24}H_{20}N_2O_8VK_2 \cdot 3(C_3H_7NO)$: C, 48.76 (49.09); H, 5.08 (5.20); N, 8.62 (8.12); V, 6.3 (6.5).

K_2VO[bencam]. This complex was prepared as above with H_4phencam, except using 0.200 g (0.46 mmol) of H_4bencam **2**, 2.5 mL of 0.50 M KOH/EtOH in 15 mL of EtOH, and 0.123 g (0.46 mmol) of $VO(acac)_2$. Recrystallization from DMF/Et_2O (trace H_2O) yielded X-ray diffraction quality crystals as large blue-green needles, 0.275 g (75%). IR (KBr pellet, cm^{-1}) 3410 (br s), 3230 (br s), 3059 (m), 2928 (m), 1662 (s), 1630 (s), 1589 (m), 1550 (s), 1490 (w), 1462 (m), 1441 (s), 1388 (m), 1298 (m), 1251 (s), 1215 (s), 1099 (m), 1059 (m), 952 (s), 745 (m), 669 (s), 640 (m), 540 (m), 407 (m). Anal. Calcd (found) for $C_{24}H_{20}N_2O_7VK_2 \cdot 3C_3H_7NO$: C, 49.74 (49.55); H, 5.19 (5.19); N, 8.79 (8.80); V, 6.4 (6.8).

X-ray Crystallographic Analysis. General Methods. The crystals were transferred to a petri dish and covered with degassed paratone N oil in the glove box. The crystals were cut from larger needles, mounted on a glass capillary in the oil and cooled under a stream of nitrogen on an Enraf-Nonius CAD-4 automated four-circle diffractometer. After centering the crystal in the beam, the cell constants were determined by least-squares treatment of 24 strong, high-angle reflections well-spaced throughout reciprocal space. The space group for both of the complexes was uniquely determined to be $P2_1/n$ (No. 14, alternate setting) on the basis of systematic absences. All data $+h,+k,\pm l$ were collected in the range 3° ≤ 2θ ≤ 45° using the ω–2θ scan technique. Orientation and intensity control reflections were monitored every 200 reflections and every hour of data collection respectively. After data collection was completed, azimuthal scans were recorded for three and four (for the phencam and bencam complexes, respectively) strong reflections with χ > 80°. Both structures were solved using the MULTAN direct methods package from Enraf-Nonius. In the final cycles of refinement, hydrogens were included in the structure factor calculations (but not refined on) at idealized positions 0.95 Å (0.87 Å for N–H distances) and with B_{iso}'s 1.25 times that of the bonded atoms. Crystal data and data collection parameters are summarized in Table I.

Table I. Summary of Crystallographic Data and Parameters for K_2[VO(1)]·3C_3H_7NO and K_2[VO(2)]3C_3H_7NO

compd	K_2[VO(1)]	K_2[VO(2)]
formula	$C_{33}H_{41}N_5O_{11}VK_2$	$C_{33}H_{41}N_5O_{10}VK_2$
fw	812.87	796.87
temp (K)	188	188
cryst system	monoclinic	monoclinic
space group (No.)	$P2_1/n$ (14)	$P2_1/n$ (14)
cell constants[a]		
a (Å)	13.644(3)	13.844(4)
b (Å)	16.643(5)	17.633(7)
c (Å)	16.753(2)	16.410(4)
β (deg)	99.13(1)	108.07(2)
Z	4	4
V (Å^3)	3756(2)	3808(4)
abs coeff, μ_{calc} (cm^{-1})	5.37	5.27
δ_{calc} (g/cm^3)	1.437	1.390
F(000)	1692	1660
cryst dimens (mm)	0.55 × 0.45 × 0.48	0.39 × 0.42 × 0.50
radiation (λ (Å))	Mo Kα (0.710 73)	Mo Kα (0.710 73)
diffractometer	Enraf-Nonius CAD-4	Enraf-Nonius CAD-4
h,k,l range collcd	0→14, 0→17, −18→17	0→14, 0→18, −17→16
2θ range	3.0–45.0	3.0–45.0
scan type	ω–2θ	ω–2θ
scan speed (θ, deg/min)	5.00	5.61
reflcns collcd	5409	5395
unique reflcns	4941	4961
reflcns with ($F_o^2 > 3\sigma(F_o^2)$)	3995	3572
no. of params	478	482
data/param ratio	8.4	7.4
$R = [\sum\|\Delta F\|/\sum\|F_o\|]$	0.036	0.051
$R_w = [\sum w(\Delta F)^2/\sum wF_o^2]$	0.043	0.066
GOF	2.563	2.308
final diff $\rho_{max}^+/\rho_{max}^-$ (e$^-$/Å^3)	+0.411[b]/−0.285	+0.709[c]/−0.109

[a] Unit cell parameters and their esd's were derived by a least-squares fitting of the setting angles of 24 reflections in the range 22.4° ≤ 2θ ≤ 25.6° and 21.2° ≤ 2θ ≤ 28.8° for K_2[VO(1)] and K_2[VO(2)], respectively. [b] Located near C30 of DMF no. 3. [c] Located near C13 of the benzene ring.

Structure Solution for K_2VO[phencam]. Upon rejection of the systematic absences and redundant data ($h0l$, $h + l \neq 2n$; $0k0$, $k \neq 2n$; $0kl$, $l \leq 0$), no decay correction was applied to the data (average loss in intensity of standard reflections was less than 1%). Azimuthal scans showed some absorption (0.96–1.00 transmission), and an empirical absorption correction was applied to the data. The positions of the vanadium, both potassiums, and most of the atoms of the catecholamide groups were located from the direct methods output. Subsequent iterations of least-squares and difference Fourier techniques revealed the remainder of the dianionic complex as well as three DMF molecules of solvation surrounding the potassium ions. Disorder of one methyl from DMF no. 2 (C30) was successfully modeled with 0.30/0.70 occupancy. After anisotropic refinement on all of the non-hydrogen atoms, C–H and N–H hydrogens were included in the structure factor calculation at idealized positions, resulting in a lowering of the R-value to 3.7%. The largest peak (e$^-$/Å^3) on the subsequent difference Fourier map was located 1.1 Å from the phenol oxygen (O8) and was included in the structure factor calculations at this position but not refined on. The six worst reflections were zero-weighted in the final cycles of refinement, and the final residuals for 478

Table II. Summary of Spectroscopic and Electrochemical Data for the Oxovanadium(IV) Complexes with Data for the $[VO(cat)_2]^{2-}$ Complex from Refs 22 (for IR and Visible Spectral Data) and 38 (for EPR Spectral Data)

compd	λ_{max} (ϵ, M^{-1} cm^{-1})[a]	$\nu_{V=O}$ (cm^{-1}) solid state[b]	$\nu_{V=O}$ (cm^{-1}) DMF soln	g_{iso} (A_{iso})[c]	g_z (A_z), $g_{x,y}$ ($A_{x,y}$)	$E^{\circ\prime}$ (V^{5+}/V^{4+})[d] (V)
$[VO(\mathbf{1})]^{2-}$	528 nm (sh), 650 nm (81)	923	961	1.974(81)	1.953(154), 1.980(52)	+0.023
$[VO(\mathbf{2})]^{2-}$	528 nm (sh), 650 nm (82)	955	961	1.974(82)	1.953(154), 1.982(52)	+0.028
$[VO(cat)_2]^{2-}$	540 nm (39), 656 nm (69)	970[e]	n.a.	1.975(82)	1.947(154), 1.981(50)	n.a.

[a] Obtained in methanol for $[VO(\mathbf{1})]^{2-}$ and $[VO(\mathbf{2})]^{2-}$, and in 0.1 M KOH for $[VO(cat)_2]^{2-}$. [b] The same values were obtained for both Nujol mulls and KBr pellets. [c] Values for A are in 10^{-4} cm^{-1}. [d] Potentials are given vs SCE in anhydrous DMF with 0.1 M Bu_4PF_6 as the supporting electrolyte. [e] Seen as a shoulder on a peak at 950 cm^{-1}.

variables refined against the 3995 data for which $F_o^2 > 3\sigma(F_o^2)$ were R = 3.6%, R_w = 4.3%, and GOF = 2.563. The R value for all data was 5.4%. The largest peak in the final difference Fourier of +0.411 $e^-/Å^3$ was located near the disordered DMF carbon, C30.

Structure Solution for K_2VO[bencam]. Upon rejection of the systematic absences and redundant data ($h0l$, $h + l \neq 2n$; $0k0$, $k \neq 2n$; $0kl$, $l \leq 0$), no decay correction was applied to the data (average change in intensity of standard reflections was +2.0%). Azimuthal scans showed some absorption (0.92–1.00 transmission), and an empirical absorption correction was applied to the data. The positions of the vanadium and the two potassiums, as well as the coordination sphere of the vanadium and several ligand atoms were located from the direct methods output. Subsequent iteratioins of least-squares and difference Fourier techniques revealed three DMF solvent molecules, two of which showed disorder. After modeling of the disorder for the solvent molecules and anisotropic refinement on all of the non-hydrogen atoms (except those of the disordered solvent), a difference Fourier map revealed the presence of hydrogens for most of the molecule at chemically meaningful positions. Hydrogens were then included in the structure factor calculation at idealized positions. The five worst reflections were zero-weighted in the final cycles of refinement, and the final residuals for 482 variables refined against 3572 data for which $F_o^2 > 3\sigma(F_o^2)$ were R = 5.1%, R_w = 6.6%, and GOF = 2.308. The R value for all data was 7.4%. The largest peak in the final difference Fourier of +0.709 $e^-/Å^3$ was situated near C13 of the benzene ring on the backbone.

Physical Measurements. Visible spectra were recorded on an HP8450A diode array spectrophotometer in 1.00-cm path-length solution cells equipped with high-vac Teflon stopcocks to facilitate sample preparation in the glove box and prevent air oxidation of the vanadyl complexes. IR spectra were recorded on a nicolet 5DXB FTIR Spectrometer equipped with a continuously nitrogen-purged sample chamber. IR spectra were obtained as either Nujol mulls on KBr plates or as KBr pellets, or in DMF solution. IR solution cells were Wilks 5320 which were matched and calibrated (0.10-mm path length) with KRS-5 (thallium–bromide/iodide) windows. The solution IR spectra were corrected for solvent bands by comparison to pure DMF, and the subtracted spectra showed no significant interference from solvent bands in the region of interest (900–1000 cm^{-1}). EPR spectra were recorded on an IBM/Bruker ER 200D-SRC instrument operating at ca. 9.4 GHz at 110 K or at ambient temperature using quartz flat cells or cylindrical tubes sealed under nitrogen. DPPH was used as an internal standard. The EPR sample solutions were prepared by one of two methods: Method 1, dropwise addition of NaOH to a slurry of the ligand and $VOSO_4$ in deoxygenated 0.1 M aqueous $KClO_4$, with DMSO added to ensure good glass formation; method 2, by dissolving the isolated complexes in anhydrous, deoxygenated EtOH or DMF. Cyclic voltammetric experiments were carried out at ambient temperature on a BAS-100A setup in anhydrous DMF (Aldrich Chemical) solution with a platinum working electrode, platinum wire auxiliary electrode, and a saturated calomel reference electrode (SCE). Experiments were performed under an inert atmosphere at 1–5 mM metal complex concentration, with 0.1 M tetrabutylammonium hexafluorophosphate ($TBAPF_6$) as the supporting electrolyte. IR compensation was achieved before each cyclic voltammogram, and the SCE reference electrode was checked by the potential of the ferrocinium/ferrocene redox couple at +0.475 V vs SCE. Spectroscopic and electrochemical data for the metal complexes are summarized in Table II.

Results and Discussion

Synthesis. The design rationale of the phencam, **1**, ligand centers around two considerations: (1) the incorporation of strongly coordinating ligands (deprotonated catecholamides) for equatorial coordination to the V(IV) center, and (2) the incorporation of a phenolic proton donor to hydrogen bond to the oxo. The tetraanionic equatorial coordination of the two deprotonated catecholamides was chosen to increase the electron density on the metal center and thus increase the basicity of the vanadyl oxygen. The two carbon chain length between the phenolic linker arm and the catecholamide function was arrived at through the inspection of CPK models to allow the phenol to sit above and within 3.0 Å of the oxo. The bencam, **2**, ligand was synthesized as a means of comparing the same ligand topology without the phenolic proton donor.

Scheme I

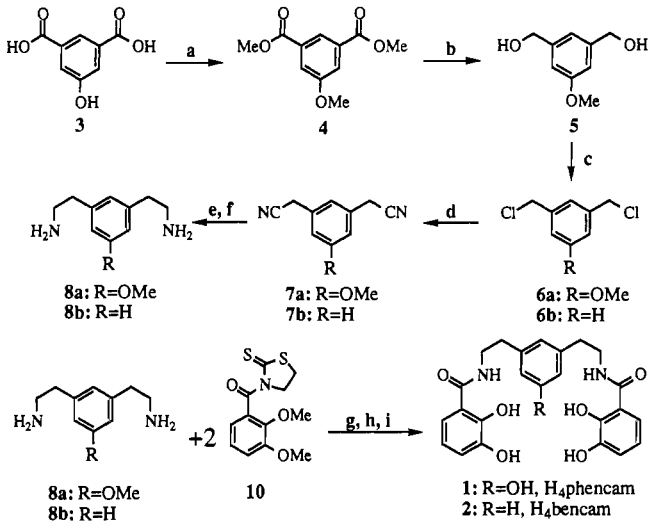

a: 3 Me_2SO_4, K_2CO_3/acetone, Δ; **b**: $LiAlH_4$/THF; **c**: 2.5 $SOCl_2$, Et_3N/CH_2Cl_2, Δ; **d**: excess KCN, cat. 18-crown-6/CH_3CN; **e**: 500 psi H_2, PtO_2/HOAc; **f**: NaOH; **g**: Et_3N/CH_2Cl_2; **h**: BBr_3/CH_2Cl_2; **i**: H_2O, Δ.

The synthesis of the phencam ligand **1** (Scheme I) was relatively straightforward: extension of the arms on the phenol linker from one to two carbons was accomplished by permethylation of the hydroxyisophthalic acid **3** with dimethyl sulfate,[26] reduction of the diester **4** to the diol **5**,[27] followed by conversion to the dichloride **6a** and subsequent conversion to the dinitrile **7a** using the "naked anion" technique.[30] The reduction of the dinitrile to the diamine **8a** was best accomplished using PtO_2 as catalyst in glacial acetic acid under >500 psi H_2.[29] Acylation of this diamine was carried out by condensation with the activated 2,3-dimethoxybenzoic acid derivative **10**[31] to give the methyl-protected ligand Me_4-phencam, **9a**. Deprotection with BBr_3 to afford the protonated ligand **1** was accomplished by standard methods for the demethylation of catechol derivatives.[32,33] The synthesis of the bencam ligand **2** required fewer steps since the dichloride **6b** is commercially available. The remainder of the steps in the synthesis of **2** were essentially identical to those used for **1** and proceeded in good to excellent yields. The ligands were synthesized in overall yields of 40% and 54% for **1** and **2**, respectively.

(30) Cook, F. L.; Bowers, C. W.; Liotto, C. L. *J. Org. Chem.* **1974**, *39*, 3416.
(31) Nagao, Y.; Miyasaka, T.; Hagiwara, Y.; Fujita, E. *J. Chem. Soc., Perkin Trans. 1* **1984**, 183 and references therein.
(32) Rodgers, S. J.; Lee, C.-W.; Ng, C. Y.; Raymond, K. N. *Inorg. Chem.* **1987**, *26*, 1622.
(33) Weitl, F. L.; Raymond, K. N. *J. Am. Chem. Soc.* **1981**, *102*, 2289.

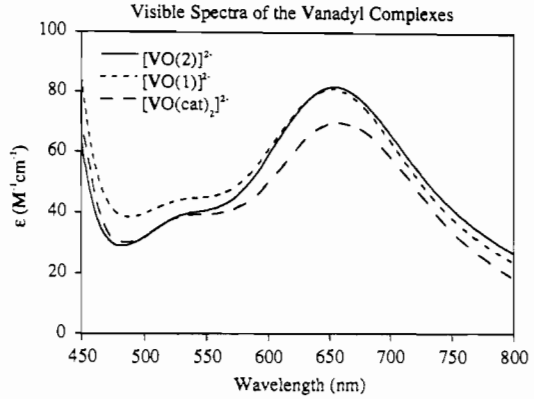

Figure 1. Visible spectra of $[VO(\mathbf{1})]^{2-}$, and $[VO(\mathbf{2})]^{2-}$ in methanol and $[VO(cat)_2]^{2-}$ in 0.1 M KOH/H_2O. The visible spectrum of the $[VO(cat)_2]^{2-}$ (from ref 22) is shown for comparative purposes.

The oxovanadium(IV) complexes of **1** and **2** were prepared under basic conditions by employing 2 equiv of ethanolic KOH[34] with $VO(acac)_2$ as the source of VO^{2+} (and the two $acac^-$ ligands to serve as the remaining base equivalents). The resultant acacH and H_2O produced in the reaction could then be removed in vacuo to afford the vanadyl complex cleanly. The resultant vanadyl complexes are oxygen sensitive in solution and in the solid state, but are stable indefinitely as solids or in solution under an inert atmosphere. A summary of the spectroscopic and electrochemical data for the $[VO(phencam)]^{2-}$ and $[VO(bencam)]^{2-}$ complexes is presented in Table II, and the results are discussed below.

Visible Spectra. The visible spectra of vanadium(IV) catecholate complexes vary characteristically from square pyramidal bis(catecholato)oxovanadium(IV) (green) to pseudo-octahedral tris(catecholato)vanadium(IV) species (dark blue). The former displays two low-intensity ($\epsilon \approx 30$–70 M^{-1} cm^{-1}) d–d transitions and the latter displays intense ($\epsilon \approx 8000$–9000 M^{-1} cm^{-1}) ligand-to-metal charge transfer (LMCT) transitions.[22] Since catecholate ligands can displace the oxo from the vanadium center (under buffered conditions), the visible spectra are a useful tool for determining whether the ligands bind as the expected bis(catecholate) species. The visible spectra of the $[VO(phencam)]^{2-}$ and $[VO(bencam)]^{2-}$ complexes, shown in Figure 1, contain two bands at 540 nm (sh) and 654 nm ($\epsilon = 82$ M^{-1} cm^{-1}) and are virtually superimposable upon the visible spectrum of $[VO(cat)_2]^{2-}$. These bands are assigned as $b_2(d_{xy}) \rightarrow b_1(d_{x^2-y^2})$ and $b_2(d_{xy}) \rightarrow e(d_{xz},d_{yz})$ transitions, respectively, assuming idealized C_{4v} symmetry at the metal center.[35-37] The two catecholamides from the bencam and phencam ligands thus bind to the oxovanadium(IV) center and the oxo group remains intact under the conditions of the synthesis.

EPR Spectra. The EPR spectra of the bis(catecholato)oxovanadium(IV) and tris(catecholato)vanadium(IV) species have been previously determined[22,38] and serve as comparisons to those of the $[VO(phencam)]^{2-}$ and $[VO(bencam)]^{2-}$ complexes. The d^1 vanadium(IV) center exhibits a characteristic eight-line EPR spectrum at ambient temperature due to hyperfine splitting of the signal by the ^{51}V nucleus ($I = {}^7/_2$). Low-temperature EPR spectra show the axial splitting pattern which is characteristic for complexes with the intact vanadyl (VO^{2+}) unit.[38] As summarized in Table II, the $[VO(phencam)]^{2-}$ and $[VO(bencam)]^{2-}$ complexes give EPR parameters similar to the bis-catecholate oxovanadium(IV) species, with $A_z > A_{x,y}$ and $g_z < g_{x,y}$ and parameters typical for catecholate coordination.[38,39] The anisotropic EPR parameters determined for the frozen samples were independent of the method of preparation of the complexes (aqueous or DMF solution). In addition, under the aqueous preparation conditions pseudo-octahedral tris(catecholamido)vanadium(IV) species were not detected.[40]

Electrochemistry. The electrochemical properties of the oxovanadium(IV) complexes of the phencam and bencam ligands were examined with cyclic voltammetry.[41] The air-sensiitive complexes were studied in argon-saturated DMF solution between +1.00 V and −1.60 V; $[VO(\mathbf{1})]^{2-}$ and $[VO(\mathbf{2})]^{2-}$ exhibit quasi-reversible oxidative waves at $E_f = +0.023$ V and +0.028 V vs SCE, respectively. The peak-to-peak separation between the waves was between 63 and 69 mV (independent of scan rate between 0.025 and 1.000 V s^{-1} and identical to the wave separation observed for the ferrocenium/ferrocene couple under the experimental conditions), and the peak current ratios (I_c/i_a) were between 0.93 and 0.99. An irreversible oxidative wave at ca. $E_{p,a} = +0.65$ V vs SCE was also observed for both complexes. Repeated scanning past the wave at +0.65 V resulted in a decrease in current density for the reversible oxidative wave near +0.02 V, as well as an increase in the cathodic to anodic wave separation for this redox couple.

The quasi-reversible redox process near +0.02 V is presumed due to an essentially metal-centered V^V/V^{IV} couple, and the irreversible oxidation at +0.65 V from the oxidation of the catecholamide ligand. The 3,5-di-*tert*-butylcatecholato complex of oxovanadium(IV) exhibits a V^V/V^{IV} irreversible redox process at a slightly lower potential of $E_{p,a} = -0.13$ V (in CH_3CN vs SCE).[42] This difference in potential is consistent with the lower electron donation of the catecholamide ligand relative to the di-*tert*-butylcatechol ligand. The electrochemical behavior of vanadium(IV)–catecholamide derivatives[43] also indicate that ligand-centered redox processes occur at potentials >+0.53 V (vs NHE), or approx. >+0.30 V vs SCE.[44] Since the terminal oxo of the VO^{2+} unit should not greatly affect the potential of a catecholamide ligand-based redox process, similar electrochemical behavior for the bencam and phencam oxovanadium(IV) complexes is expected. The irreversible oxidative wave at $E_{p,a} = +0.65$ V is thus assigned to a catecholamide-based redox process similar to other catechols.[42,45,46]

General Structural Descriptions of $K_2[VO(\mathbf{1})]$ and $K_2[VO(\mathbf{2})]$. The single-crystal X-ray structures of $K_2[VO(\mathbf{1})]$ and $K_2[VO(\mathbf{2})]$ show that both are composed of discrete complex dianions (Figure 2) which are linked by a complex network of potassium counterions and solvent molecules (three DMF's of solvation). Positional and thermal parameters and distances and selected angles for the two complexes are shown in Tables III–VI. The

(34) Other strong bases can be substituted for the ethanolic KOH employed in the synthesis described here, including tetraalkylammonium hydroxides. However, if less than two equivalents of base are employed in the synthesis problems arise with the productiion of dark blue species, characteristic of vanadium(IV) in an octahedral environment (e.g., tris(catecholato)vanadium(IV)). These species would presumably be due to oligomer formation, with concomitant displacement of the vanadyl oxygen.

(35) Ballhausen, C. J.; Gray, H. B. *Inorg. Chem.* **1962**, *1*, 111.

(36) Selbin, J. *Chem. Rev.* **1965**, *65*, 153.

(37) Selbin, J. *J. Coord. Chem. Rev.* **1966**, *1*, 293.

(38) Branca, M.; Micera, G.; Dessi, A.; Sanna, D.; Raymond, K. N. *Inorg. Chem.* **1990**, *29*, 1586.

(39) Chasteen, N. D. In *Biological Magnetic Resonance*; Berliner, L. J., Reuben, J., Eds.; Plenum Press: New York, 1981; Vol. 3.

(40) This is in contrast to less rigid long-chain alkyl triamine-linked bis(catecholamide) ligands, for which tris(catecholate) pseudo-octahedral vanadium(IV) species have been detected under the identical preparation conditions for the EPR experiments: Dewey, T. M. Ph.D. Thesis, University of California at Berkeley, 1992.

(41) See the Experimental Section for details of the electrochemical setup.

(42) Bosserman, P. J.; Sawyer, D. T. *Inorg. Chem.* **1982**, *21*, 1545.

(43) Bulls, A. R.; Pippin, C. G.; Hahn, F. E.; Raymond, K. N. *J. Am. Chem. Soc.* **1990**, *112*, 2627.

(44) This is the potential for the V(V)/V(IV) couple for a tris(catecholamide)-coordinated vanadium center. The ligand oxidation occurs at a significantly higher potential.

(45) Stallings, M. D.; Morrison, M. M.; Sawyer, D. T. *Inorg. Chem.* **1981**, *20*, 2655.

(46) It should be noted that the oxidation of di-*tert*-butylcatecholate–metal complexes can also lead to reversible formation of semiquinone–metal complexes. See, for example: (a) Battacharya, S.; Boone, S. R.; Fox, G. A.; Pierpont, C. G. *J. Am. Chem. Soc.* **1990**, *112*, 1088. (b) deLearie, L. A.; Haltiwanger, C.; Pierpont, C. G. *J. Am. Chem. Soc.* **1989**, *111*, 2292 and references therein.

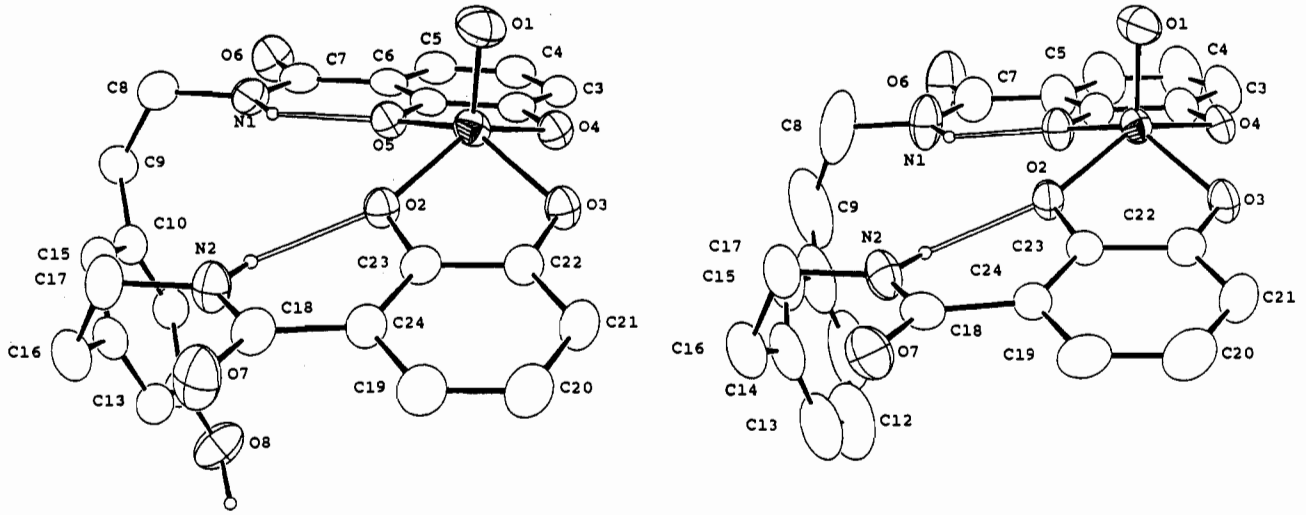

Figure 2. ORTEP diagrams of the $[VO(1)]^{2-}$ complex (left) and $[VO(2)]^{2-}$ complex (right) showing the orientation of the linking phenol or benzene ring relative to the coordination sphere of the oxovanadium(IV). Ellipsoids are drawn at the 50% probability level.

remaining distances and angles for the K^+ coordination spheres as well as the intramolecular angles for the ligands are provided as supplementary material.

The two complexes are very similar in coordination geometry and ligand conformation. In both complexes the benzene or phenol linking arm is pointing away from the coordination of the VO^{2+} precluding the desired intramolecular hydrogen bond for the phencam complex. In both cases the benzene linking arm is tilted at an angle of about 65–70° relative to the plane of equatorial coordination. The VO^{2+} resides in a square pyramidal geometry, surrounded in the equatorial plane by the two bidentate catecholamide ligands and at the apex by the oxo. There is no significant distortion toward trigonal bipyramidal geometry, as demonstrated by the trans O_{eq}–V–O_{eq} angles of 141.3(1)°/145.5(1)° for $[VO(1)]^{2-}$ and 145.3(1)°/141.8(1)° for $[VO(2)]^{2-}$.[47,48] The vanadium atom sits 0.61(1) Å above the plane of equatorial coordination formed by the four catecholamide oxygens for both $[VO(1)]^{2-}$ and $[VO(2)]^{2-}$. Similar to what was seen for the bis(catecholato)oxovanadium(IV) complex,[22] the two catechol rings are bent down and away from the oxo group; the planes described by the catechol rings thus make angles of 157.4(1)° and 161.2(1)°, as compared to 156.4(1)° for the analogous dihedral angle for $[VO(cat)_2]^{2-}$. The amide N–H of each catecholamide is hydrogen-bonded to the catechol oxygens, forming six-membered rings. The planes described by amide functions O=C–N are essentially coplanar with the catechol ring: for $[VO(1)]^{2-}$ these dihedral angles are 3(2)° and 11.9(5)°, and for $[VO(2)]^{2-}$ these angles are 4.6(9)° and 10.1(4)°. This type of strong hydrogen bonding from the catecholamide functions has been seen with transition-metal catecholamide and 2,3-dihydroxyterephthalamide complexes,[49-52] This hydrogen-bonding constrains the catechol rings, the amide functions, and the methylene carbon attached to the amide nitrogen to be essentially coplanar. The vanadium atom sits slightly out of the plane described by the catechol (0.332(1) Å and 0.337(1) Å for $[VO(1)]^{2-}$, and 0.351(1) Å and 0.387(1) Å for $[VO(2)]^{2-}$, and the dihedral angles between the catechol rings and the corresponding chelate O–V–O planes are 13.5(2)° and 13.2(3)° for $[VO(1)]^{2-}$ and 14.3(2)° and 16.1(3)° for $[VO(2)]^{2-}$.

The similarity between the $[VO(1)]^{2-}$ and $[VO(2)]^{2-}$ complexes is further illustrated in Figure 3, in which is shown an overlay of the two complexes. The rms error which results from the overlay is 0.143 Å for all of the analogous non-hydrogen atoms (i.e., all except the phenol [O8] of the phencam ligand); and if only the catechol rings and vanadium coordination spheres are overlaid, the rms error which results is only 0.057 Å.

Hydrogen Bonding to the Oxo Atom. The previous discussion has focused on the similarities between the solid state structures of $[VO(1)]^{2-}$ and $[VO(2)]^{2-}$. However, one difference can be seen by closer inspection of the packing of the molecules: the phenol arm of the $[VO(1)]^{2-}$ complex, although bent down relative to the vanadyl oxo, is hydrogen-bonded to the vanadyl oxo of a neighboring complex (Figure 4, left). The individual $[VO(1)]^{2-}$ complexes are linked via hydrogen bonds between the oxo (O1) oxygens and the phenol (O8) in an infinite chain along the 2_1-screw axis of the unit cell. A closer view of the resultant *inter*molecular hydrogen-bond geometry is shown in Figure 4, right.

The phenol proton was located 1.561(2) Å from O1 and 1.131(2) Å from the O8 as the largest peak of a difference Fourier map after inclusion of the remaining hydrogens in the structure factor calculations at calculated positions (vide supra). The vanadyl oxo (O1) to phenol oxygen (O8) distance is 2.612(4) Å. As a comparison, the O–O distance in ice is 2.75 Å and the sum of the van der Waals radii for oxygens is 2.80 Å. Location of the proton (H-O8) allows an estimate of the strength of the hydrogen bond. Hydrogen bonds (O–H···O type) with O–O distances between 2.8 and 3.0 Å are considered weak, and those with O–O distances between 2.6 and 2.8 Å (the majority) are considered relatively strong, ca. 15–40 kJ/mol.[21] The near linearity of the O–H···O angle (151.5(2)°) and the V=O···H angle (149.4(2)°) also support the notion that this hydrogen bond is similar to those observed in organic structures, for example organic structures where the amide carbonyl serves as the hydrogen bond acceptor.[53,54]

The effect of the *inter*molecular hydrogen bond is illustrated by the change in the solid-state IR spectra of the two complexes (Table II); $\nu_{V=O}$ is shifted from 955 cm^{-1} for $K_2[VO(2)]$ to 923 cm^{-1} for $K_2[VO(1)]$. A shift in the bond stretching frequency for the vanadyl V=O is consistent with a slight weakening of the bond, which would be expected upon the dipolar interaction of

(47) Muetterties, E. L.; Guggenberger, L. J. *J. Am. Chem. Soc.* **1974**, *96*, 1748.
(48) Orioli, P. L. *Coord. Chem. Rev.* **1971**, *6*, 285.
(49) McMurry, T. J.; Hosseini, M. W.; Garrett, T. M.; Hahn, F. E.; Reyes, Z. E.; Raymond, K. N. *J. Am. Chem. Soc.* **1987**, *109*, 7196.
(50) Karpishin, T. B.; Stack, T. D. P.; Raymond, K. N. *J. Am. Chem. Soc.* **1993**, *115*, 182.
(51) Karpishin, T. B.; Dewey, T. M.; Raymond, K. N. *J. Am. Chem. Soc.* **1993**, *115*, 1842.
(52) Dewey, T. M.; Raymond, K. N. *Inorg. Chem.*, to be submitted for publication.
(53) Taylor, R.; Kennard, O. *Acc. Chem. Res.* **1984**, *17*, 320.
(54) Taylor, R.; Kennard, O.; Versichel, W. *Acta Crystallogr. B* **1984**, *40*, 280.

Table III. Positional Parameters and B Values (Å^2) for Non-Hydrogen Atoms in $K_2VO[\mathbf{1}]\cdot 3C_3H_7NO$

atom	x	y	z	B(iso)[a]
V	0.19196(4)	0.21317(3)	0.12922(3)	2.37(1)
K1	0.14653(5)	0.03125(5)	0.00213(4)	2.73(2)
K2	0.23625(5)	0.25614(5)	–0.07045(4)	2.87(2)
O1	0.1967(2)	0.3065(1)	0.1026(1)	3.62(6)
O2	0.3063(1)	0.1838(1)	0.2105(1)	2.32(5)
O3	0.2680(1)	0.1543(1)	0.0590(1)	2.46(5)
O4	0.0758(1)	0.1666(1)	0.0641(1)	2.60(5)
O5	0.1096(1)	0.2044(1)	0.2139(1)	2.45(5)
O6	–0.1219(2)	0.2166(2)	0.3535(1)	3.97(6)
O7	0.5953(2)	0.1585(2)	0.3415(1)	4.03(6)
O8	0.1805(2)	–0.0944(2)	0.4512(2)	4.34(6)
O9	–0.0338(2)	0.0423(2)	–0.0999(1)	3.76(6)
O10	0.2032(2)	0.4381(2)	0.4328(2)	4.43(6)
O11	0.2101(2)	0.1010(2)	–0.1344(1)	3.80(6)
N1	0.0424(2)	0.2242(2)	0.3543(2)	2.80(6)
N2	0.4330(2)	0.1718(2)	0.3502(2)	2.98(6)
N3	–0.0333(2)	0.0791(2)	–0.2302(2)	3.06(7)
N4	0.1295(3)	0.4287(2)	0.3015(2)	6.4(1)
N5	0.2365(2)	0.0610(2)	–0.2592(2)	3.40(7)
C1	0.0139(2)	0.1899(2)	0.1842(2)	2.27(7)
C2	–0.0055(2)	0.1692(2)	0.1012(2)	2.41(7)
C3	–0.1011(2)	0.1525(2)	0.0637(2)	2.65(7)
C4	–0.1788(2)	0.1564(2)	0.1087(2)	2.81(8)
C5	–0.1606(2)	0.1756(2)	0.1892(2)	2.95(8)
C6	–0.0644(2)	0.1924(2)	0.2292(2)	2.44(7)
C7	–0.0501(2)	0.2117(2)	0.3171(2)	2.76(7)
C8	0.0656(3)	0.2474(2)	0.4386(2)	3.28(8)
C9	0.0729(2)	0.1777(2)	0.4973(2)	3.21(8)
C10	0.1540(2)	0.1190(2)	0.4872(2)	2.65(7)
C11	0.1326(2)	0.0394(2)	0.4717(2)	2.84(8)
C12	0.2067(2)	–0.0153(2)	0.4629(2)	2.84(8)
C13	0.3038(2)	0.0108(2)	0.4668(2)	2.88(8)
C14	0.3279(2)	0.0907(2)	0.4825(2)	2.62(7)
C15	0.2522(2)	0.1437(2)	0.4932(2)	2.76(7)
C16	0.4338(2)	0.1197(2)	0.4895(2)	3.37(8)
C17	0.4488(2)	0.1908(2)	0.4358(2)	3.12(8)
C18	0.5073(2)	0.1578(2)	0.3082(2)	2.77(8)
C19	0.5518(2)	0.1141(2)	0.1765(2)	2.93(8)
C20	0.5307(2)	0.0977(2)	0.0960(2)	3.05(8)
C21	0.4352(2)	0.1106(2)	0.0540(2)	2.67(7)
C22	0.3630(2)	0.1400(2)	0.0939(2)	2.16(7)
C23	0.3835(2)	0.1559(2)	0.1776(2)	2.14(7)
C24	0.4790(2)	0.1427(2)	0.2201(2)	2.41(7)
C25	–0.0246(3)	0.0926(2)	–0.1521(2)	3.55(9)
C26	–0.0195(3)	0.1428(3)	–0.2859(3)	5.2(1)
C27	–0.0557(4)	0.0007(3)	–0.2622(3)	6.7(1)
C28	0.1332(3)	0.4346(2)	0.3791(3)	4.3(1)
C29	0.0406(4)	0.4210(3)	0.2419(3)	8.0(1)
C30	0.2122(5)	0.4567(5)	0.2636(4)	7.4(2)
C30′	0.2365(9)	0.362(1)	0.2987(9)	6.8(4)
C31	0.2107(3)	0.0499(2)	–0.1876(2)	3.78(9)
C32	0.2314(4)	–0.0031(3)	–0.3184(2)	5.5(1)
C33	0.2663(3)	0.1396(3)	–0.2829(2)	5.0(1)

[a] The thermal parameter given for anisotropically refined atoms is the isotropic equivalent thermal parameter defined as $(4/3)[a^2B(1,1) + b^2B(2,2) + c^2B(3,3) + ab(\cos\gamma)B(1,2) + ac(\cos\beta)B(1,3) + bc(\cos\alpha)B(2,3)]$, where a–c are real cell parameters and $B(i,j)$ are anisotropic β's.

Table IV. Positional Parameters and B Values (Å^2) for Non-Hydrogen Atoms in $K_2VO[2]\cdot 3C_3H_7NO$

atom	x	y	z	B(iso)[a]
V	0.06630(6)	0.16223(4)	–0.01268(5)	2.24(2)
K1	0.02517(8)	0.05467(6)	0.38402(7)	3.26(2)
K2	–0.00132(8)	0.02696(6)	0.13137(6)	3.00(2)
O1	0.1116(2)	0.1616(2)	0.0900(2)	3.24(8)
O2	0.1460(2)	0.2306(2)	–0.0613(2)	2.41(7)
O3	0.1380(2)	0.0853(2)	–0.0570(2)	2.65(7)
O4	–0.0484(2)	0.0909(2)	–0.0390(2)	2.44(7)
O5	–0.0452(2)	0.2362(2)	–0.0502(2)	2.70(7)
O6	–0.3089(3)	0.3667(2)	–0.0793(3)	5.9(1)
O7	0.3873(2)	0.3432(2)	–0.1167(2)	3.99(8)
O8	0.0826(3)	–0.0499(2)	0.2780(2)	3.82(9)
O9	0.0645(3)	0.0678(2)	0.5640(3)	5.3(1)
O10	–0.0074(4)	0.1309(3)	0.2360(3)	4.9(1)*
O10′	–0.0728(9)	0.1183(7)	0.2112(7)	4.1(3)*
N1	–0.1471(3)	0.3677(2)	–0.0782(3)	4.2(1)
N2	0.2292(3)	0.3546(2)	–0.1078(3)	3.2(1)
N3	0.1608(3)	–0.1639(2)	0.3106(3)	4.0(1)
N4	0.0881(4)	0.1774(3)	0.6399(3)	5.1(1)
N5	–0.0406(5)	0.2507(4)	0.2000(4)	4.9(2)*
N5′	–0.096(1)	0.2422(8)	0.1807(8)	3.3(3)*
C1	–0.1355(3)	0.2061(3)	–0.0542(3)	2.6(1)
C2	–0.1380(3)	0.1269(3)	–0.0471(3)	2.6(1)
C3	–0.2265(4)	0.0891(3)	–0.0507(3)	3.8(1)
C4	–0.3140(4)	0.1308(4)	–0.0612(4)	5.3(2)
C5	–0.3135(4)	0.2077(4)	–0.0681(4)	4.7(2)
C6	–0.2254(4)	0.2479(3)	–0.0661(3)	3.5(1)
C7	–0.2309(4)	0.3316(3)	–0.0751(4)	3.9(1)
C8	–0.1443(5)	0.4499(3)	–0.0865(5)	6.8(2)
C9	–0.1729(6)	0.4762(4)	–0.1799(6)	8.5(2)
C10	–0.1003(5)	0.4574(3)	–0.2275(5)	6.1(2)
C11	–0.1355(5)	0.4305(4)	–0.3107(5)	7.8(2)
C12	–0.0696(6)	0.4170(4)	–0.3561(5)	8.6(2)
C13	0.0329(6)	0.4288(4)	0.3205(4)	6.8(2)
C14	0.0716(5)	0.4551(3)	–0.2373(4)	4.7(1)
C15	0.0035(5)	0.4698(3)	–0.1928(4)	5.2(2)
C16	0.1825(5)	0.4707(3)	–0.1965(4)	4.9(2)
C17	0.2292(4)	0.4363(3)	–0.1091(3)	3.8(1)
C18	0.3110(3)	0.3134(3)	–0.1082(3)	2.8(1)
C19	0.3802(3)	0.1844(3)	–0.1130(3)	3.2(1)
C20	0.3755(3)	0.1066(3)	–0.1089(3)	3.6(1)
C21	0.2956(4)	0.0713(3)	–0.0896(3)	3.2(1)
C22	0.2198(3)	0.1137(3)	–0.0735(3)	2.5(1)
C23	0.2237(3)	0.1947(3)	–0.0773(3)	2.3(1)
C24	0.3036(3)	0.2295(3)	–0.0893(3)	2.4(1)
C25	0.1084(4)	–0.1112(3)	0.2588(3)	4.1(1)
C26	0.1928(6)	–0.1521(5)	0.4014(4)	7.5(2)
C27	0.1837(7)	–0.2376(4)	0.2797(5)	9.1(2)
C28	0.0610(7)	0.1365(5)	0.5651(6)	4.4(2)
C29	0.1362(7)	0.1294(7)	0.7200(6)	5.7(3)
C30	0.086(1)	0.2573(6)	0.6434(9)	9.0(4)
C28′	0.094(1)	0.108(1)	0.646(1)	5.9(4)
C29′	0.048(2)	0.227(1)	0.561(1)	8.4(6)
C30′	0.091(2)	0.228(1)	0.719(1)	7.8(6)
C31	0.0279(6)	0.1954(5)	0.2356(5)	4.2(2)*
C32	0.008(1)	0.3260(8)	0.1962(8)	9.4(3)*
C33	–0.156(1)	0.2407(8)	0.1651(8)	10.0(4)*
C31′	–0.133(2)	0.176(2)	0.183(2)	7.8(7)*
C32′	–0.133(2)	0.306(2)	0.154(2)	8.6(7)*
C33′	0.017(1)	0.258(1)	0.219(1)	4.0(4)*

[a] Starred B values are form atoms that were included with isotropic thermal parameters. The thermal parameter given for anisotropically refined atoms is the isotropic equivalent thermal parameter defined as $(4/3)[a^2B(1,1) + b^2B(2,2) + c^2B(3,3) + ab(\cos\gamma)B(1,2) + ac(\cos\beta)B(1,3) + bc(\cos\alpha)B(2,3)]$, where a–c are real cell parameters, and $B(i,j)$ are anisotropic β's.

the lone pair(s) of the oxo oxygen with the phenol proton 1.56 Å distant. There is no sixth coordination from another complex anion or a solvent heteroatom trans to the oxo which could be responsible for this weakening of the V=O bond. Interactions of the oxo with the potassium cations can also be ruled out as the cause of this shift in the stretching frequency.[55]

The differences in the V=O stretching frequencies seen in the solid state IR spectra of $[VO(\mathbf{1})]^{2-}$ and $[VO(\mathbf{2})]^{2-}$ disappear in DMF solution (Table II), and the $\nu_{V=O}$ for both complexes is 961 cm^{-1}. This is consistent with the $[VO(\mathbf{1})]^{2-}$ complex being monomeric and not hydrogen-bonded, either *intra*- or *inter*molecularly, in DMF solution. This observation also confirms the similarity in coordination environments the phencam and bencam ligands provide in the absence of the hydrogen bond in the solid state.

(55) In the hydrogen-bonded phencam complex the vanadyl oxo does participate in a somewhat weak interaction with the K2 counterion; the K2–O(oxo) distance is 3.15 Å, as compared to average K2–O distances of 2.77 Å (to amide carbonyl oxygens from solvent DMF molecules or from symmetry-related ligand molecules). In the non-hydrogen-bonded $[VO(\mathbf{2})]^{2-}$ complex however, the vanadyl oxo is located slightly closer to a potassium counterion, at 2.97 Å from K2 (the average K2–O distances are 2.76 Å). This is inconsistent with the observation that the bencam complex has a stronger V=O bond and higher stretching frequency then the hydrogen-bonded phencam complex.

Table V. Selected Intra- and Intermolecular Distances (Å) in $K_2VO[1]\cdot 3C_3H_7NO$ and $K_2VO[2]\cdot 3C_3H_7NO$

K_2VO[phencam]		K_2VO[bencam]	
V–O1	1.620(2)	V–O1	1.606(3)
V–O2	1.963(2)	V–O2	1.963(3)
V–O3	1.951(2)	V–O3	1.949(3)
V–O4	1.938(2)	V–O4	1.965(3)
V–O5	1.950(2)	V–O5	1.968(3)
$V–O_{eq}$(av)	1.951(2)	$V–O_{eq}$(av)	1.961(3)
O1–O8	2.612(4)		
O1–H–O8	1.561(2)		
O8–H–O8	1.131(2)		
O2–C23	1.346(4)	O2–C23	1.343(6)
O3–C22	1.356(3)	O3–C22	1.341(5)
O4–C2	1.355(4)	O4–C2	1.363(6)
O5–C1	1.343(3)	O5–C1	1.344(6)
O6–C7	1.235(4)	O6–C7	1.228(6)
O7–C18	1.242(4)	O7–C18	1.225(6)
O8–C12	1.369(4)		
N1–C7	1.333(4)	N1–C7	1.339(7)
N1–C8	1.449(4)	N1–C8	1.459(8)
N2–C17	1.452(4)	N2–C17	1.441(7)
N2–C18	1.343(4)	N2–C18	1.349(7)
C1–C2	1.417(4)	C1–C2	1.401(7)
C1–C6	1.402(5)	C1–C6	1.407(7)
C2–C3	1.384(4)	C2–C3	1.380(7)
C3–C4	1.397(5)	C3–C4	1.384(8)
C4–C5	1.370(5)	C4–C5	1.358(9)
C5–C6	1.404(4)	C5–C6	1.401(8)
C6–C7	1.490(5)	C6–C7	1.483(8)
C8–C9	1.513(5)	C8–C9	1.537(12)
C9–C10	1.506(5)	C9–C10	1.491(13)
C10–C11	1.372(5)	C10–C11	1.379(12)
C10–C15	1.390(5)	C10–C15	1.391(9)
C11–C12	1.385(5)	C11–C12	1.360(13)
C12–C13	1.387 (5)	C12–C13	1.378(12)
C13–C14	1.385(5)	C13–C14	1.382(10)
C14–C15	1.392(5)	C14–C15	1.382(9)
C14–C16	1.510(5)	C14–C16	1.496(9)
C16–C17	1.521(5)	C16–C17	1.505(8)
C18–C24	1.486(4)	C18–C24	1.496(7)
C19–C20	1.362(5)	C19–C20	1.375(8)
C19–C24	1.406(5)	C19–C24	1.405(7)
C20–C21	1.395(4)	C20–C21	1.388(7)
C21–C22	1.365(5)	C21–C22	1.379(7)
C22–C23	1.411(4)	C22–C23	1.431(7)
C23–C24	1.401(4)	C23–C24	1.398(6)

Table VI. Intra- and Intermolecular Angles (deg) around the Vanadium(IV) Coordination Spheres in $K_2VO[1]\cdot 3C_3H_7NO$ and $K_2VO[2]\cdot 3C_3H_7NO$

$K_2VO[1]$		$K_2VO[2]$	
O1–V–O2	111.56(10)	O1–V–O2	110.2(2)
O1–V–O3	105.50(11)	O1–V–O3	108.0(2)
O1–V–O4	107.3(10)	O1–V–O4	104.5(2)
O1–V–O5	108.94(11)	O1–V–O5	110.2(2)
av O1–V–O_{eq}	108.3(11)	av O1–V–O_{eq}	108.2(2)
O2–V–O3	81.57(8)	O2–V–O3	82.0(1)
O2–V–O4	141.31(9)	O2–V–O4	145.3(1)
O2–V–O5	87.90(8)	O2–V–O5	87.2(1)
O3–V–O4	85.72(9)	O3–V–O4	86.8(1)
O3–V–O5	145.49(9)	O3–V–O5	141.8(1)
O4–V–O5	82.26(9)	O4–V–O5	81.6(1)
V–O2–C23	112.92(17)	V–O2–C23	112.1(3)
V–O3–C22	113.03(18)	V–O3–C22	112.1(3)
V–O4–C2	112.64(18)	V–O4–C2	111.9(3)
V–O5–C1	112.53(19)	V–O5–C1	112.4(3)
V–O1–O8	139.15(14)		
V–O1–H–O8	149.38(17)		
O1–H–O8–O8	151.52(15)		

The other effect of the hydrogen bond is somewhat more subtle but consistent with the observed IR spectral differences between the two complexes. The V=O bond length changes from 1.606(3) Å for $[VO(2)]^{2-}$ to 1.620(2) Å for $[VO(1)]^{2-}$, and the average

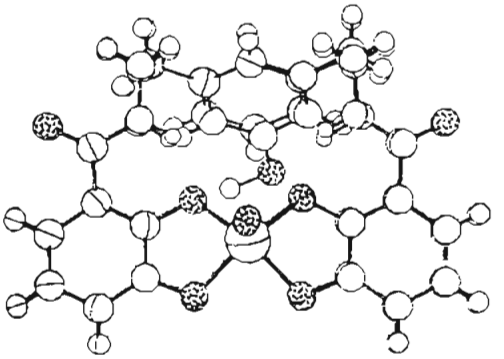

Figure 3. Overlay view of $[VO(1)]^{2-}$ with $[VO(2)]^{2-}$ showing the similarities in the ligand conformation. The rms error for all of the non-hydrogen atoms of the molecules (excluding the phenol oxygen O8) is 0.143 Å.

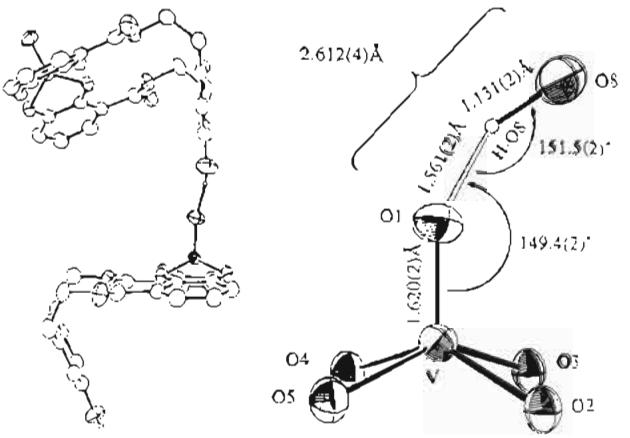

Figure 4. ORTEP diagram of the two symmetry-related $[VO(1)]^{2-}$ complexes showing the intermolecular hydrogen bond (left) and a detail of the coordination sphere and the geometry around the hydrogen bond between the phenol (O8) and the oxo (O1) (right). Thermal ellipsoids are drawn at the 50% probability level.

$V–O_{eq}$ distances are 1.961(3) Å and 1.951(2) Å for the respective complexes. That is, the V=O bond length increases and the $V–O_{eq}$ bond lengths decrease upon hydrogen-bonding to the oxo; each difference is significant on the basis of statistical tests established by Cruickshank and Robertson.[56] Collectively they are consistent with the donation of electron density from the oxo to the phenol proton in the structure of $K_2[VO(1)]$. This effect is similar to that observed for the weakening of the $\nu_{V=O}$ with more electron-donating equatorial ligands.[57]

Summary and Conclusions

In the first step toward the design of ligands which are capable of two-point binding to the metal oxo unit, we have examined the coordination chemistry of prototypical ligands. These are based on two bidentate catecholamide units (to bind strongly to the vanadium(IV) center) and a phenol linking arm (to *intra*molecularly hydrogen bond to the oxo atom). Two related oxovanadium(IV) complexes have been characterized: the hydrogen-bonded $[VO(1)]^{2-}$ and its non-hydrogen-bonded control $[VO(2)]^{2-}$. The presence of the hydrogen bond in the solid-state structure of $K_2[VO(1)]$ (albeit intermolecular) supports the general ligand design approach; it results in a substantial decrease in the V=O IR stretching frequency, which is consistent with a dipolar interaction of the phenolic proton with the oxo group. In addition, the solid-state structures exhibit bond-length differences between the two complexes which are consistent with a weakening of the V=O bond and an increase in the interaction of the equatorial

(56) Cruickshank, D. W. J.; Robertson, A. P. *Acta Cryst.* **1953**, *6*, 698.
(57) Selbin, J.; Holmes, L. H., Jr.; McGlynn, S. P. *J. Inorg. Nucl. Chem.* **1963**, *25*, 1359.

ligands with the vanadium center. These spectroscopic and structural data are important for the analysis or assessment of future ligand designs.

Other ligand design modifications are suggested by the two structures. In the $[VO(\mathbf{1})]^{2-}$ complex the phenol arm is bent down and inward. Since the catecholamide ring and the amide function are constrained to be essentially planar, the nitrogen to alkyl carbon bond is directed away from the coordination sphere around the vanadium, and hence away from the oxo group. The first alkyl carbon atoms are ca. 6.3 Å from and are oriented perpendicular to the vanadyl moiety (V=O- -C is <90°). To bring the proton donor to within 3 Å and nearly axial to the vanadyl (V=O–X ≈ 180°) requires architecture which was not anticipated in the first generation of ligands. Ongoing work is aimed at the design of ligands which incorporate macrocyclic or macrobicyclic or other such restrictive structures, as well as different ligand sets which allow for the attachment of proton donors in more geometrically accessible positions.

Acknowledgment. The authors gratefully acknowledge the National Science Foundation for financial support (NSF CHE-8919207), and T.M.D. for a graduate fellowship. We thank Daniele Sanna for assistance with the EPR characterization.

Supplementary Material Available: Tables of hydrogen atom positions and anisotropic thermal parameters for non-hydrogen atoms (Tables VIIS–XS), remaining bond angles for the complex dianions $[VO(\mathbf{1})]^{2-}$ and $[VO(\mathbf{2})]^{2-}$ (Tables XIS and XIIS), and bond distances and angles for the potassium coordination spheres (Tables XVS and XVIS), unit cell packing diagrams for the two complexes (Figure 5S), and text describing the synthesis of the bicam ligands based on polyamine backbones and precursors to these ligands (15 pages). Ordering information is given on any current masthead page.